Numerical analysis of reaction kinetic accompanying flow and dispersion in structured ZSM-5@SiC open-cell foam catalyst

Peng Yan[a] | Qiuyan Ding[a] | Jing Zou[b] | Jian Na[a] | Xueli Geng[a] | Hong Li[a] | Xin Gao[a,c,*]

[a]*School of Chemical Engineering and Technology, Tianjin University, National Engineering Research Center of Distillation Technology, Collaborative Innovation Center of Chemical Science and Engineering (Tianjin), Tianjin 300072, China*

[b]*The State Key Laboratory of Precision Measuring Technology and Instruments, Tianjin University, Tianjin 300072, China*

[c]*Haihe Laboratory of Sustainable Chemical Transformations, Tianjin 300192, China*

* Corresponding author's Email, gaoxin@tju.edu.cn (X. Gao)

Abstract

Chaotic flow inside porous media accelerates the transport, mixing, and reaction of molecules and particles in widespread natural and factitious processes. Current macroscopic models based on the average pore-scale variations show obvious limitations in the prediction of many chemical processes. In this paper, we reconstruct microscopic foam structures using Micro Computed Tomography to simulate fluid flow in structured ZSM-5@SiC foam catalyst. Moreover, we propose a conceptual model based on the microscopic mean square displacement theory to characterize the effective dispersion inside an open-cell foam. This model will explain the flow characteristics of confined fluid inside the porous media from fluid elements perspective. Particularly, dispersion factor and structure factor, as key parts of this model, perfectly interpret the driving characteristics of pressure drop, velocity different, and reaction in continuous foam media flow. This work also provides a

unique means of predicting reaction kinetics of confined fluid in structured foam catalyst.

Keywords: open-cell foam, dispersion, CFD, μ-CT reconstruction, surface reaction

1. Introduction

Flow and dispersion in open-cell foams endow this cellular medium with outstanding radial heat transfer [1], radial mixing [2], and low-pressure loss [3], thus being considered attractive structured catalyst support to enhance external transport-limited catalytic processes, such as column internals for reactive distillation [4], wastewater disinfection and removal of contaminants [5,6], Fischer-Tropsch synthesis [7], preferential oxidation of CO in hydrogen-rich gas [8], catalytic wet peroxide oxidation [9], improvements in methanol-to-propylene (MTP) reactions [10]. However, the flow and dispersion of the internal fluid have not been well defined due to the complex strut structure of open-cell foams, which limits the comprehensive understanding of the mixing, transport, and reaction kinetics inside porous channels.

Until now, the macroscopic Reynolds number [11] is usually used to define the flow characteristics inside porous media, and the most critical is the parameter of the characteristic length and velocity inside porous media. Ideally, the particle diameter (d_{par}), pore diameter (d_p), or integral length scale (d_I) is considered the characteristic length. The mean velocity of the perpendicular to the flow direction is taken as the intrinsic mean velocity (**U**) (Re_p in Equation 1). While Ergun [12] used hydraulic diameter (d_H) as characteristic length (Re_H in Equation 2). Later Dybbs & Edwards [13] uses Darcy's superficial velocity instead of intrinsic mean velocity to define the Reynolds number (Re_D in Equation 3). Next, Kaviany [14] corrected the Reynolds number based on the Darcy permeability, κ (Re_κ in Equation 4). However, these models define the flow regime based on the

average velocity, while ignoring the inhomogeneity of velocity value and the variation of velocity direction in the porous medium. This is indeed reasonable for uniform porous channels, but it is insufficient for complex channel distributions, especially foam channels. This time-averaged form cannot show the stretching and folding of fluid elements [15] caused by velocity differences inside the foam channels. However, the exponential deformation of such fluid elements would enhance micro-scale chemical gradients and pore-scale incomplete mixing [16]. Therefore, it is very meaningful to comprehensively define the fluid flow and dispersion in open-cell foam substrates based on microscopic models, which will help to further understand the mixing, transport, and reaction kinetics inside the foam channels.

$$\mathrm{Re}_p = \frac{\rho \|\mathbf{U}\| d_p}{\mu} = \frac{\|\mathbf{U}\| d_p}{\nu} \tag{1}$$

$$\mathrm{Re}_H = \frac{\rho \|\mathbf{U}\| d_H}{\mu} = \frac{2}{3}\left(\frac{\varepsilon}{1-\varepsilon}\right)\frac{\rho \|\mathbf{U}\| d_p}{\mu} = \frac{2}{3}\left(\frac{\varepsilon}{1-\varepsilon}\right)\mathrm{Re}_p \tag{2}$$

$$\mathrm{Re}_D = \frac{\varepsilon\rho \|\mathbf{U}\| d_p}{\mu} = \frac{\varepsilon \|\mathbf{U}\| d_p}{\nu} = \varepsilon \cdot \mathrm{Re}_p \tag{3}$$

$$\mathrm{Re}_\kappa = \sqrt{\kappa}\,\frac{\rho \|\mathbf{U}\| d_p}{\mu} = \sqrt{\frac{\varepsilon^3}{180(1-\varepsilon)^2}}\,\frac{\rho \|\mathbf{U}\| d_p}{\mu} \tag{4}$$

In the microscopic model, we may consider a flowing fluid to consist of the aggregations of material elements small enough to satisfy the requirements to treat the fluid as a continuum [17]. We know that even in quite small containers, it takes a long time to achieve homogeneity by molecular diffusion alone without convection. Therefore, this process is accelerated by convection. Turbulence, as the most classic form of convection, triggers the Kolmogorov energy cascade [18,19], which rapidly creates small-scale structures in the spatial distribution of advected fields to achieve homogeneity.

While the porous medium divides the space into three-dimensional connected small-scale structures through the obstacles such as particles and struts, so that the internal fluid elements are stretched and folded, and then the homogeneity is quickly achieved (Chaotic advection). Compared to disordered turbulent structures, chaotic advection does not require high Reynolds numbers, can be achieved in laminar flow regimes, and flow paths can be defined depending on the porous structure. For example, Heyman et al.[15] defined the dimensionless stretching rate and found that the average dimensionless stretching rate for random granular media (d_{par} = 7, 10, and 20 mm) was 0.21 and the mixing efficiency was 3.1%, a value comparable to industrial mixers [20]. This is an order of magnitude higher than 0.45% for a microfluidic mixer with a staggered herringbone channel [21]. Therefore, it is very necessary to define the flow and dispersion through the movement locus of the fluid elements in the foam medium and then make the reference for transport, mixing and reaction inside foam media.

The fluid flow path in the foam channel is very dependent on the structural characteristics of the foam. The common foam media such as metal, SiC, polymer, etc. are not optically matched. It is difficult to experimentally capture the motion trajectories of fluid elements in foam media. With the development of computational fluid dynamics (CFD) and tomography reconstruction technology [22], it is possible to simulate the flow [2,3,23-25], dispersion [26], heat transfer [1,27], and reaction [28-30] inside the foam channel. Such as Bracconi [3] explore virtually-generated foam models and their 3D printed replicas for a combined CFD and experimental study of fluid dynamics in foams. Fan [26] simulated the fluid flow in a realistic SiC foam model and found that the dispersion coefficient of laminar flow within foams was estimated at 10^{-4} $m^2 \bullet s^{-1}$, which is much larger than the molecular

dispersion coefficient in a typical laminar flow in an open channel. The above studies have shown that it is very reliable to simulate the movement of fluid elements in the channels under laminar flow conditions based on real foam structures. This is also the more attractive research method to investigate the flow, dispersion, and reaction inside the foam channel.

Therefore, in this paper, based on micro-computed tomography (μ-CT), the realistic open-cell foam structure was reconstructed, and it was used as a structured catalyst (ZSM-5@SiC) to simulate the effects of porosity (55% < ε < 75%), mean pore diameter (0.6 mm < d_p < 1.9 mm), flow velocity (22 < Re < 73), molar ratio of LA to EtOH (1/3 < R_m < 2/1) and temperature (340.15 K < T < 356.15 K) on the catalytic esterification. In addition, the flow and dispersion characteristics of fluid elements inside the channel are defined based on the microscopic mean square displacement theory. A conceptual model was developed to explain the flow characteristics in the foams from the perspective of fluid elements, and the characteristic parameters in this model perfectly reflected the pressure drop, velocity difference, and conversion of LA in the structured ZSM-5@SiC open-cell foam catalyst.

2. Experimental equipment and process

A circulating plug flow reactor with an inner diameter of 20 mm and a length of 370 mm was designed and set up, as shown in Figure 1, to conduct the experiments [31,32]. It is equipped with 7 sections of D = 20 mm, H = 50 mm structured ZSM-5@SiC catalyst as shown in Figure 1(d) (For details of ZSM-5@SiC, please refer to the work of Ding et al. [31]). Stainless steel pipes with ribbon heater were connected to the material tank, pump, and reactor. The constant temperature of silicone oil is passed into the jacket of the reactor and the material tank to control the reaction temperature.

The temperature error is controlled by ± 0.1 K. The feed was fed into the reactor uniformly from the bottom through a plunger pump (J-X40/1.5). The top product is further returned to the material tank to be recirculated into the reactor. The total feed amount in this experiment was approximately 200 mL to ensure that there was no reaction liquid in the material tank during the cycle, which was helpful to distinguish the residence time of the circulating material in the reaction section and the non-reaction section. Every 30 minutes, samples were taken from the top outlet to analyze the molar composition of the mixed liquid. When the composition was unchanged, the reaction was stopped. Finally, the above steps were repeated and the kinetic data under different operating conditions were determined.

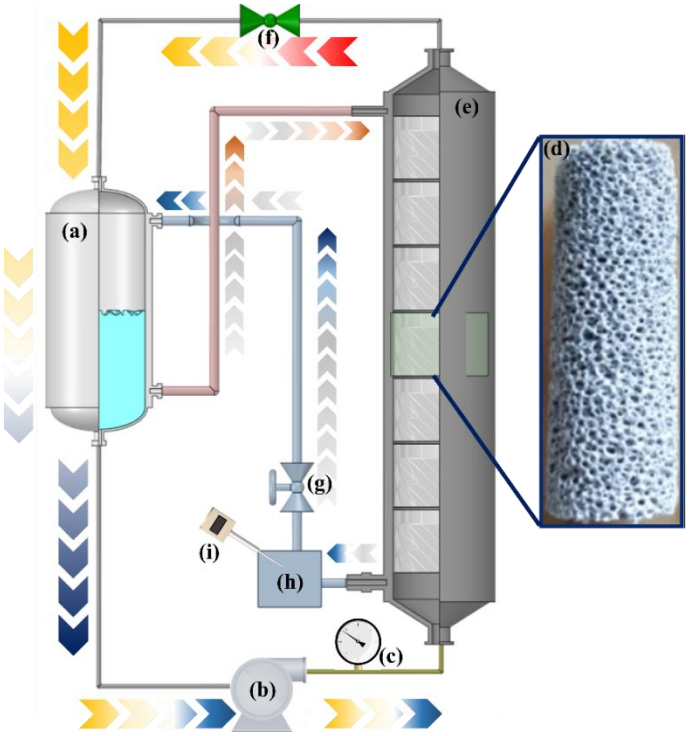

FIGURE 1 Experimental setup (a) material tank; (b) plunger metering pump; (c) flowmeter; (d) ZSM-5@SiC catalyst; (e) tubular reactor; (f) valve; (g) circulating pump;(h) circulating silicone oil; (i) thermometer.

3. Geometric model

3.1 Scan the foam structure

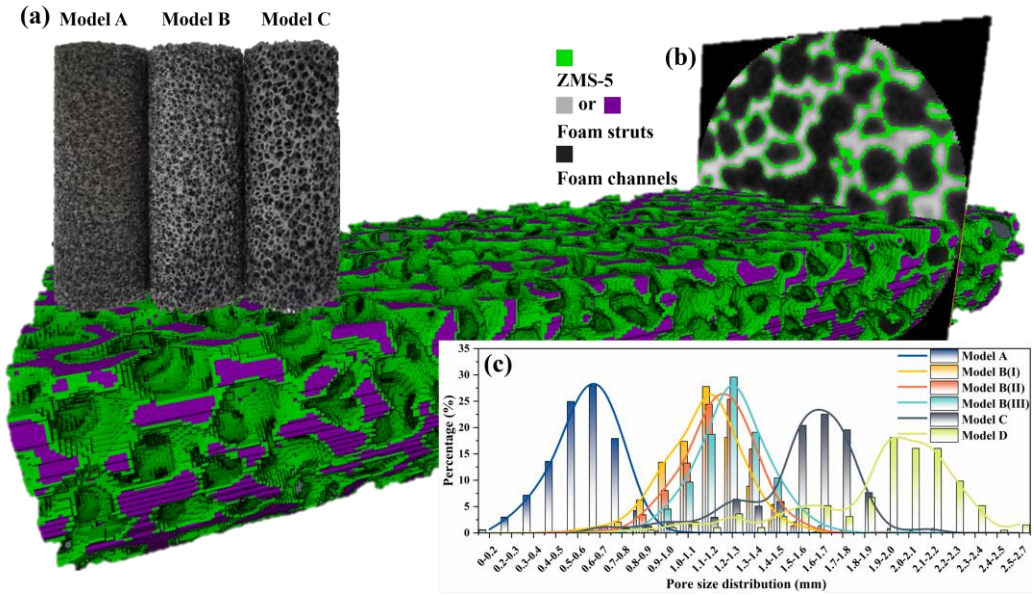

FIGURE 2 (a) The front view of foam substrate without ZMS-5 coating; (b) The reconstruction of foam substrates (Model C) by X-ray CT (green: ZMS-5, grey or purple: foam struts, black: foam channels); (c) Pore size distribution of different foam structures.

In this paper, SiC foam materials were supplied by the Institute of Metal Research, Chinese Academy of Science [33]. Four pore sizes of SiC foam structures were selected as the research objects, and their real structures without ZSM-5 catalyst are shown in Figure 2(a). The ZSM-5@SiC catalysts (Foam materials coated with ZSM-5) with different structures were subjected to Micro Computed Tomography (μ-CT, which was jointly developed by Tianjin University and Tianjin Sanying Precision Instrument Co., Ltd, the highest scanning voltage is 160 kV, the maximum power is 25W, and the highest resolution is 0.5μm.). Layer-by-layer structural images of the foam material obtained by μ-CT were analyzed using Avizo software. Then, the internal solid regions (in Figure 2(b), foam strut are grey or purple regions, catalyst is green region) and fluid regions (in Figure 2(b), foam channels are black regions) were obtained by identifying the foam strut, catalyst, and pores layer by layer, as shown in Figure 2(b). Based on the center of the foam structure as the center of the circle, a foam structure with a radius of 3 mm and a height of 10 mm was selected as the research object. Moreover, we adopted a segmentation method based on the difference of gray image values

to segment the solid and fluid domains. Models A, B(I), B(II), B(III), C, and D were established by adjusting the segmentation threshold, and their initial porosity was 65%, 55%, 65%, 75%, 65%, and 65%. Figure 2(c) shows the pore size distribution of these models obtained by spheroid-like analysis of the pore cells in the selected foam structure.

3.2 Reconstructing the foam structure

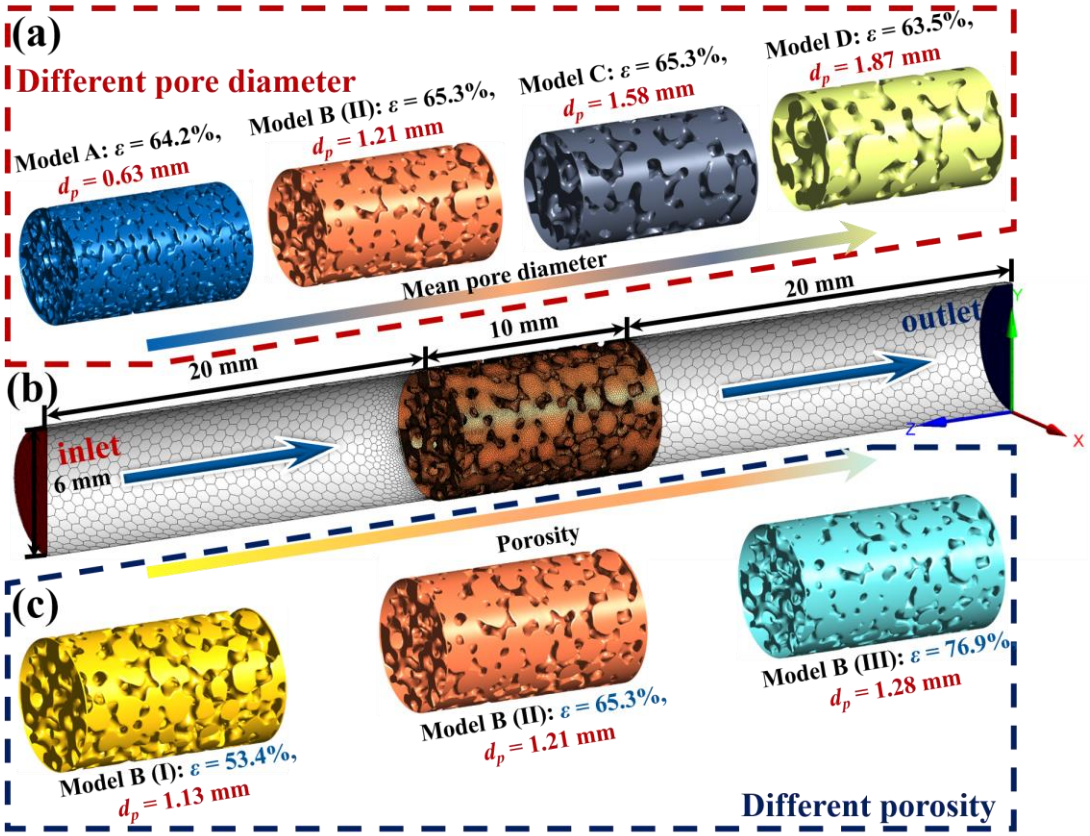

FIGURE 3 (a) Detailed information of foam structure with different mean pore size; (b) Geometric model and detailed dimensions; (c) Detailed information of foam structure with different porosity.

Next, the reconstructed 3D real foam column was imported into SPACECLAIM to establish a fluid domain as shown in Figure 3(b). The length of the whole fluid domain is 50 mm, the foam medium is placed in the middle, the length is 10 mm, the diameter of the channel (d_c) is 6 mm, and the velocity inlet and pressure outlet are 20 mm away from the foam medium. Then this fluid domain was import in FLUENT MESHING to refine and smooth the internal rough foam channels, the

optimized models are shown in Figures 3(a) and 3(c). The porosity and mean pore size of the Models A, B(I), B(II), B(III), C, and D is 64.2% & 0.63 mm, 53.4% & 1.13 mm, 65.3% & 1.21 mm, 76.9% & 1.28 mm, 65.3% & 1.58 mm, and 63.5% & 1.78 mm, respectively. Figure 3a shows different pore diameters with similar porosity (the foam structure without a catalyst is model A, B, and C in Figure 2(a)). Figure 3(c) shows different porosity with similar pore diameters (the foam structures without catalyst are all model B in Figure 2(a)). In addition, the reason for selecting this foam size as a representative elementary volume in this paper is as follows: (i) there are no two absolutely identical foam structures, and exploring the foam structure with larger size (>10 cm) is not conducive to calculation (mesh with poor quality or large number). (ii) the size of foam selected in this research can completely show the difference of flow rules caused by different foam structures (pore size distribution and porosity). (iii) the effects of foam structure on dispersion, flow, pressure drop, velocity difference and conversion rate were investigated. See section 5 for detailed discussion.

4. Numerical simulation method

4.1 Mathematical model

The simulation in this paper adopts the finite volume method, and its mass, momentum, and energy equations are as follows:

Mass equation:

$$\frac{\partial \rho}{\partial t} + \nabla \cdot \left(\rho \mathbf{u} \right) = 0 \tag{5}$$

Momentum equation:

$$\frac{\partial}{\partial t}\left(\rho \mathbf{u} \right) + \nabla \cdot \left(\rho \mathbf{u}\mathbf{u} \right) = \nabla P + \nabla \left(\mu_{eff} \left(\nabla \mathbf{u} + \nabla \mathbf{u}^{T} \right) \right) + \rho \mathbf{g} \tag{6}$$

Energy equation:

$$\frac{\partial}{\partial t}(\rho E)+\nabla\cdot(\rho \mathbf{u}E)=\nabla(P\mathbf{u})+\nabla\left(\mu_{eff}\left(\nabla\mathbf{u}+\nabla\mathbf{u}^{T}\right)\mathbf{u}\right)+\rho\mathbf{g}\mathbf{u}+\nabla\cdot(\lambda_e\nabla T)+S_h-\nabla\sum_i h_i\mathbf{J}_i \tag{7}$$

where λ_e is the effective conductivity, $\vec{J}_j$ is the diffusion flux of species. S_h includes volumetric heat sources and the heat generation rate from chemical reactions shown in Equation 8.

$$E=h-\frac{P}{\rho}+\frac{u^2}{2} \tag{8}$$

where sensible enthalpy h is defined for ideal gases as Equation 9

$$h=\sum_i Y_i h_i=\sum_i Y_i\int_{T_{ref}}^{T} c_{p,i}dT \tag{9}$$

where Y_i is the mass fraction of species i, for the pressure-based solver T_{ref} is 298.15 K.

Species transport equations

$$\frac{\partial}{\partial t}(\rho Y_i)+\nabla\cdot(\rho\mathbf{u}Y_i)=-\nabla\cdot\mathbf{J}_i+R_i+S_i \tag{10}$$

where R_i is the net rate of production of species i by chemical reaction, and S_i is the rate of creation by addition from the dispersed phase plus any user-defined sources. $\mathbf{J}_i$ is the diffusion flux of species i, which is derived from gradients of temperature and concentration. This paper uses the Fick's law to model mass diffusion due to concentration gradients in laminar flows, the diffusion flux can be written as

$$\mathbf{J}_i=-\rho D_{i,m}\nabla Y_i-D_{T,i}\frac{\nabla T}{T} \tag{11}$$

where $D_{i,m}$ is the mass diffusion coefficient for species i in the mixture, and $D_{T,i}$ is the thermal diffusion coefficient. Diffusion coefficient in mixtures was calculated using kinetic theory (Chapman-Enskog formula) [34], as follows

$$D_{i,j} = 0.00188 \frac{\left[T^3 \left(\frac{1}{M_{w,i}} + \frac{1}{M_{w,j}} \right) \right]^{1/2}}{p_{abs} \sigma_{ij}^2 \Omega_D} \tag{12}$$

where $M_{w,i}$ is the molecular weight of species *i*, p_{abs} is the absolute pressure; σ_{ij} is the Lennard-Jones collision diameter in Angstroms (L-J Characteristic Length). Ω_D is a measure of the interaction of the molecules in the mixture. Ω_D is also known as the diffusion integral is a function of the quantity T_D^*, as follows

$$T_D^* = \frac{T}{(\varepsilon/k_B)_{ij}} = \frac{T}{\sqrt{(\varepsilon/k_B)_i (\varepsilon/k_B)_j}} \tag{13}$$

where k_B is the Boltzmann constant (1.38×10^{-23} J/molecule-K), which is defined as the gas constant (R) divided by Avogadro's number. ε/k_B is the Lennard-Jones potential well depth in Kelvins (L-J Energy Parameter).

For a binary mixture, σ_{ij} in Equation 12 is calculated as the arithmetic average of the individual

$$\sigma_{ij} = \frac{1}{2}\left(\sigma_i + \sigma_j\right) \tag{14}$$

Based on the finite-rate model, each species j checked by aspen corresponds to the standard state enthalpy h_j^0 and standard state entropy s_j^0 under specific conditions, and the mixing enthalpy and entropy are obtained respectively based on Equations 15 and 16.

$$H = \sum_j Y_j \left[\frac{h_j^0}{M_j} + \int_{T_{ref,j}}^{T} c_{p,j} dT \right] \tag{15}$$

$$S = \sum_j Y_j \left[\frac{s_j^0}{M_j} + \int_{T_{ref,j}}^{T} \frac{c_{p,j}}{T} dT \right] \tag{16}$$

where M_j is the molecular weight of the j^{th} species with units of kg/kmol and $T_{ref,j}$ is the

reference temperature at which s_j^0 or h_j^0 is defined.

4.2 Kinetic parameters

The net source of chemical species *i* due to reaction is computed as the sum of the reaction sources over the N_R reactions that the species participate in:

$$R_i = M_{w,i} \sum_{r=1}^{N_R} R_{i,r} \tag{17}$$

where $M_{w,i}$ is the molecular weight of species *i* and $R_{i,r}$ is the molar rate of creation/destruction of species *i* in reaction *r*. Reaction may occur in the continuous phase at wall surfaces of foam. Consider the r^{th} reaction written in general form as follows:

$$\sum_{i=1}^{N} \nu_{i,r}^{'} \zeta_i \underset{k_{b,r}}{\overset{k_{f,r}}{\rightleftharpoons}} \sum_{i=1}^{N} \nu_{i,r}^{''} \zeta_i \tag{18}$$

where, N is number of chemical species in the system, $\nu_{i,r}^{'}$ is stoichiometric coefficient for reactant *i* in reaction *r*, $\nu_{i,r}^{''}$ is stoichiometric coefficient for product *i* in reaction *r*, ζ_i is symbol denoting species *i*, $k_{f,r}$ is forward rate constant for reaction *r*, $k_{b,r}$ ($k_{b,r} = k_{f,r} / K_e$) is backward rate constant for reaction *r*.

The esterification reaction of LA with EtOH was selected in this work, and the detailed reaction equation is shown in Equation 19.

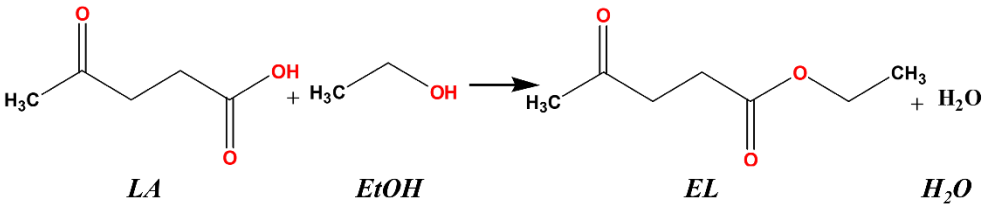

(19)

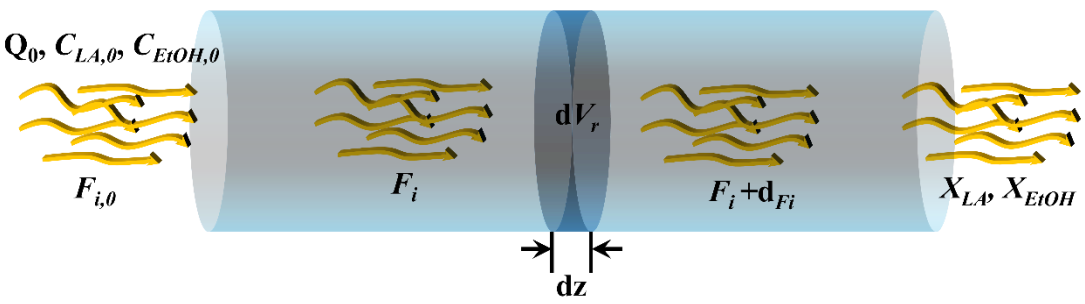

FIGURE 4 Schematic diagram of plug flow reaction

The reaction experimental equipment can be assumed to be an isothermal circulation plug flow reactor. Since the species concentration of the plug flow reactor varies with the axial direction, the micro-element volume dV_r is taken as the control volume, as shown in Figure 4. That is, the specie balance of LA satisfies the following Equation 20:

$$F_{LA} + \mathrm{d}F_{LA} - F_{LA} = R_{LA}\mathrm{d}V_r \tag{20}$$

Simplifying Equation 20 yields the following Equation 21:

$$\frac{\mathrm{d}F_{LA}}{\mathrm{d}V_r} = Q_0 \frac{\mathrm{d}c_{LA}}{\mathrm{d}V_r} = R_{LA} \tag{21}$$

Assuming that V_r is small enough, for the same reaction system, its $\frac{dc_{LA}}{dV_r}$ is the same, and when the flow rate is Q_1, its reaction kinetics satisfies the following equation (See the supporting information for detailed derivation):

$$R_{LA}^{'} = Q_1 \frac{\mathrm{d}c_{LA}}{\mathrm{d}V_r} = \frac{Q_1}{Q_0} \cdot Q_1 \frac{\mathrm{d}c_{LA}}{\mathrm{d}V_r} = \frac{Q_1}{Q_0} \cdot \left(k_{f,r} c_{LA} c_{EtOH} - k_{f,r} c_{EL} c_{H_2O} / K_e \right) \tag{22}$$

where Q_0 = 3.5 L/h, $k_{f,r}$ is the forward rate constant for catalyzed esterification, K_e is the equilibrium constant. $k_{f,r}$ is obtained based on the Model B (I) with minimum porosity 53.4% (in Equation 23, the relationship between the rate constant and the reaction temperature is shown in Figure S1), and K_e is obtained from our group previous works[35] (in Equation 24).

$$k_{f,r} = A \cdot \exp\left(-\frac{E_a}{RT} \right) = 1.2774 \times 10^6 \exp\left(-\frac{79436.1}{RT} \right) \tag{23}$$

$$K_e = 285.59 \exp\left(-\frac{13587.6}{RT} \right) \tag{24}$$

where A, and E_a units are respectively $kmol/\left(m^3 \cdot s\right)$ and $kJ/kmol$.

Flow rate is a key factor in the kinetics of the plug flow reactor. In this paper, Equation 22 is used to simulate the catalytic reaction process using the foam substrate, and to explore the influence mechanism of the fluid flow and dispersion characteristics in the foam on the reaction kinetics.

4.3. Boundary conditions and simulation details

In this paper, the fluid inside the porous channel is regarded as an ideal fluid, and the interaction between molecules in the fluid is ignored. Mass diffusivity and thermal diffusion coefficient adopt kinetic theory. Volume-weighted mixing law is used to calculate mixing density. Mass-weighted mixing law is used to calculate mixing viscosity and thermal conductivity. The mixing law is used to calculate specific heat. Moreover, we adopt velocity inlet, pressure outlet, and no-slip wall as boundary conditions. A certain premixed molar ratio of levulinic acid (LA) and ethanol (EtOH) enters through the velocity inlet, and when they touch the surface of the foam cell, the reaction is triggered to generate ethyl levulinate (EL), which flows out through the pressure outlet. The detailed simulation conditions are shown in Table 1.

Table 1

FLUENT simulation conditions

	Simulation settings
Liquid velocity inlet	0.0235-0.07 m/s
Pressure outlet	101.325 kPa
Operating pressure	101.325 kPa
Operating temperature	340.15 K-356.15 K

The surface reaction model is based on the wall surface module in the volume reaction model. As shown in Figure 2, it can be found that the catalyst is evenly coated to the surface of the foam

struts, so the foam wall surface is simplified as a catalyst coating. When the premixed reactants contact the wall surface of the foam channel, the esterification reaction is triggered. Moreover, The 'diffusion' number adopted in the section 4 of this paper is the parameter in the mixture, which is based on the properties of the liquid. The 'dispersion' in section 5 refers to the flow form of reactants in the foam channel, which is completely dependent on the foam structure and inlet flow velocity. The two are essentially different. The former is molecular scale, and the latter is fluid element scale.

5. Results and discussion

5.1. Grid independence

The main purpose of this case is to explore the effect of the flow in open-cell structured foam catalyst on catalytic reaction process. Therefore, the pressure drop, velocity, and conversion of LA inside the open-cell foam are the important targets of this research. In this paper, the cases with mesh numbers of 1,344,223, 2,753,705, and 4,044,877 are explored. The foam structure adopts model B (II), the inlet Reynolds number is 51, and the molar ratio of LA to EL is 1:1. The simulation results are shown in Figure 5. The difference of the three meshes is the size, the size of the coarse mesh is 0.07 mm - 0.3 mm, the size of the medium mesh is 0.05 mm - 0.3 mm, and the size of the fine mesh is 0.04 mm - 0.2 mm, and its detailed structure is shown in Figure 5a. Firstly, the XZ contour of pressure drop, velocity, and LA's conversion are established. It can be found that the mesh refinement has no obvious effect on the accuracy of the simulation results (in Figure 5b-d). In addition, extracting the pressure drop, the velocity, and conversion of LA at the center of the foam column. The results show that the refinement of coarse mesh to fine mesh has negligible effect on pressure drop and velocity, but the coarse mesh shows a significant error in the conversion of LA

compared with the medium mesh and fine mesh (in Figure 5d). However, the results of the medium mesh and the fine mesh are consistent in conversion of LA. Comprehensively considering the calculation efficiency and calculation accuracy, the medium mesh is finally adopted as the best meshing method. Moreover, this method is also used to mesh other foam structures, all of which have good applicability.

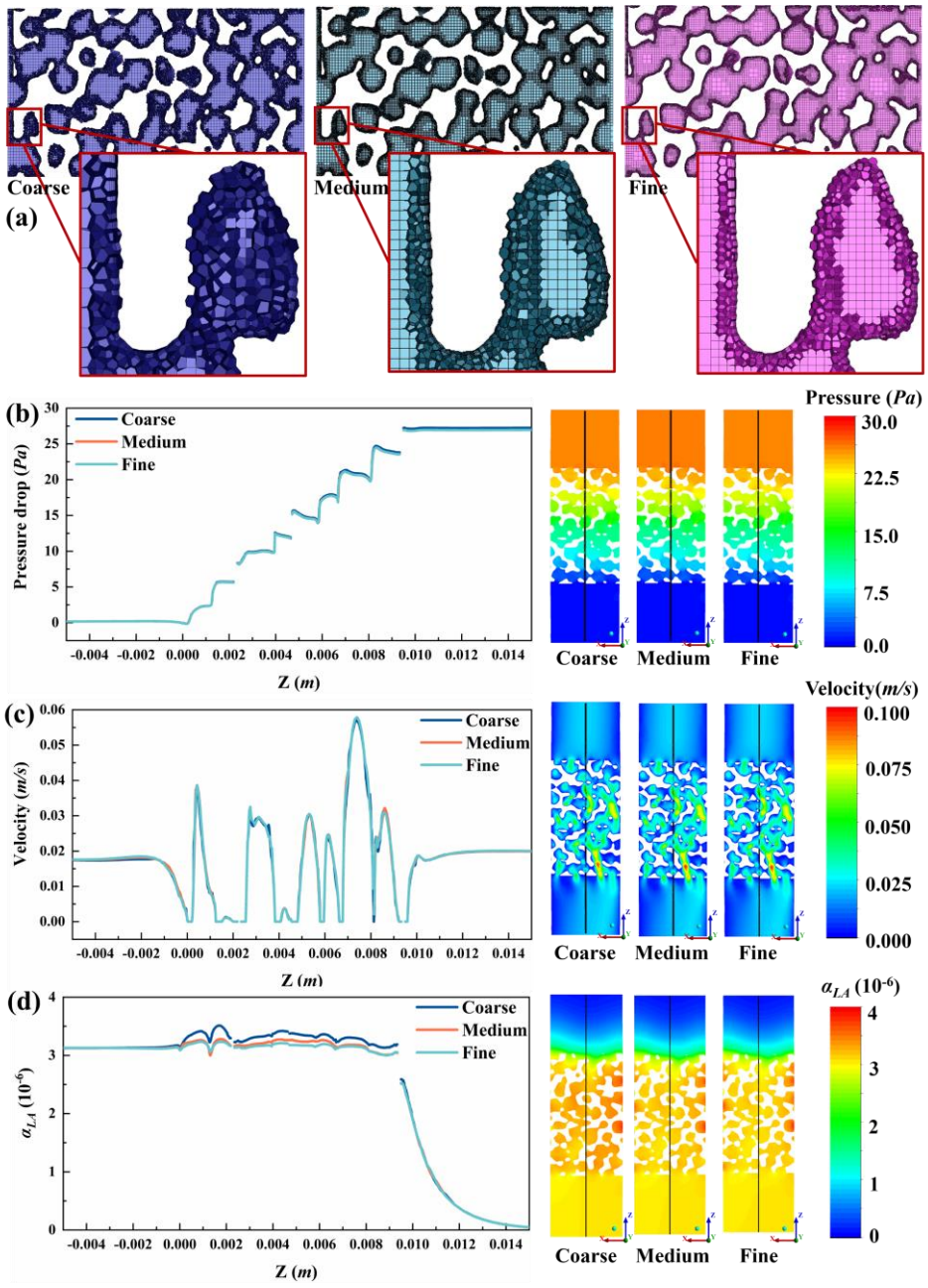

FIGURE 5 (a) Detailed mesh information with Model B (II) 65.3% (Coarse number: 1344223, Medium number: 2753705, Fine number: 4044877); (b) Distribution of pressure drop at the

centerline in different mesh count; (c) Distribution of liquid velocity at the centerline in different mesh count (d) Distribution of conversion of LA at the centerline in different mesh count.

5.2 Experimental results and model validation

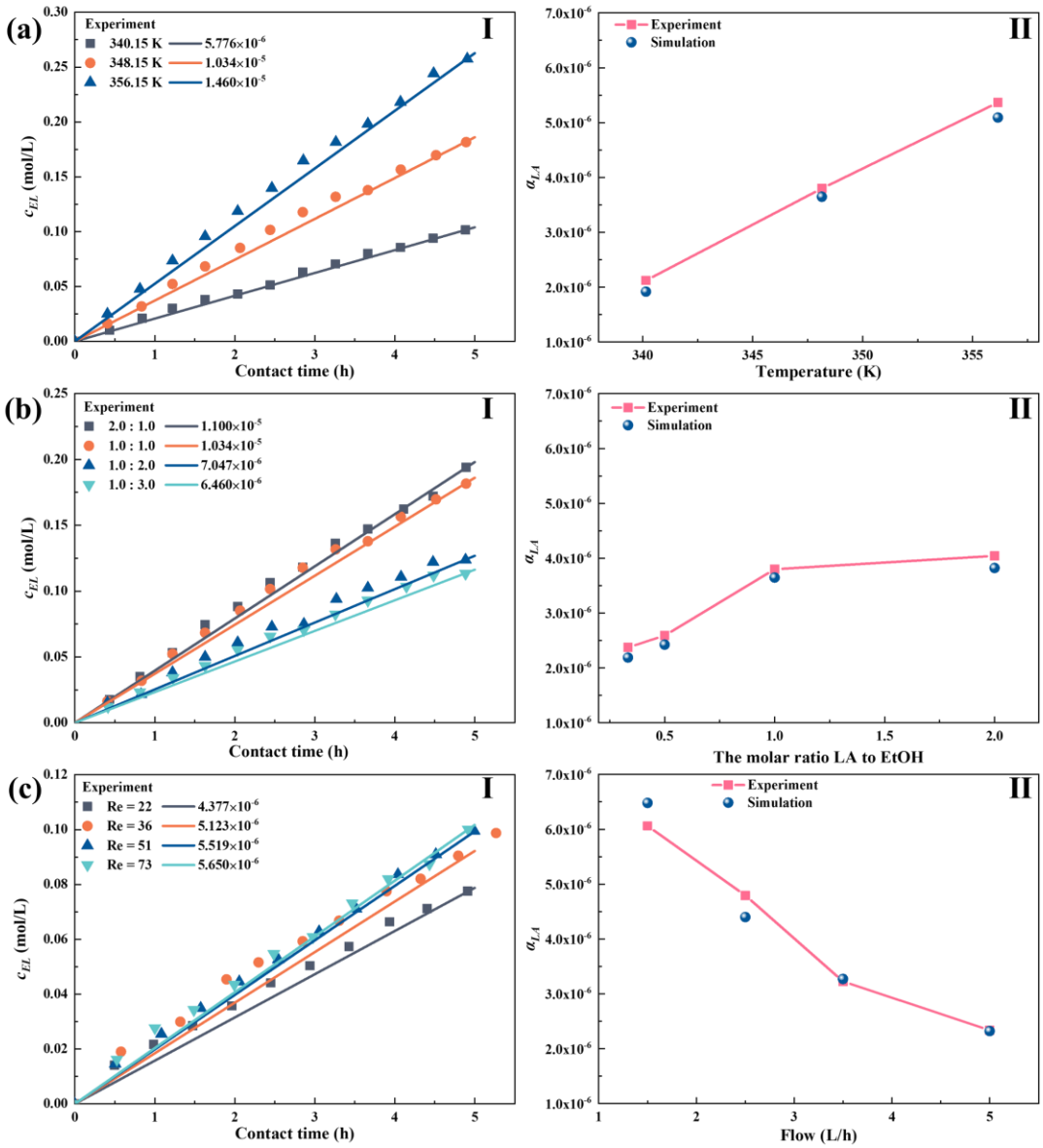

FIGURE 6 The influence of various factors on the (I) EL's molar concentration (within 5 h) and (II) conversion of LA (10 mm long foam structure, 0.2 s < t < 1.5 s): (a) Temperature; (b) The molar ration of LA to EtOH (R_m); (c): Reynolds number.

The abscissa of Figure 6 (I) is the contact time, that is, the residence time of the fluid in the reactor during the cycle. The ordinate is the molar concentration of EL. While the mark is the experimental result [31], the line is the optimal reaction rate k based on the experimental result (in Equation 5). Based on the k value, the conversion of LA in each period can be calculated and used

as a verification of the simulation results. Transient simulation of fluid flow in real foam channels is very inefficient and time-consuming. In addition, fluid flow in the foam substrate is a laminar flow region with a low Reynolds number, which can maintain a steady state. Therefore, this paper adopts steady-state calculation, when the internal flow field is stable, the EL's molar concentration at the outlet is detected, and the conversion of LA is calculated based on Equation 26. The mean residence time of the fluid inside the foam channel is obtained through the simulated data, and the EL's molar concentration in the consuming same time is calculated by Equation 25. The experimental LA's conversion was calculated according to Equation 26. The comparison of the experimental and simulation results is shown in Figure 6(II). We can find that the simulation results are consistent with the experimental results under different T, R_m, Re, and porous structures (d_p and ε). The error between the simulation and the experimental results is less than 10%. Therefore, the simulated results of the plug flow reaction kinetic model based on the realistic foam structure is reliable.

$$k = \frac{\Delta c_{EL}}{\Delta t} = \frac{c_{EL,t} - 0}{t - 0} \tag{25}$$

where k is the reaction rate, and Δc_{EL} is the variation in molar concentration of EL over time Δt.

$$\alpha_{LA} = \frac{c_{LA,0} - c_{LA,t}}{c_{LA,0}} = \frac{c_{EL,t}}{c_{LA,0}} \tag{26}$$

where α_{LA} is the molar conversion of LA, $c_{LA,0}$ is the initial molar concentration of LA, $c_{LA,t}$ and $c_{EL,t}$ are the molar concentrations of LA and EL at time t.

5.3 The frequency distribution of D_α and α with porous structure

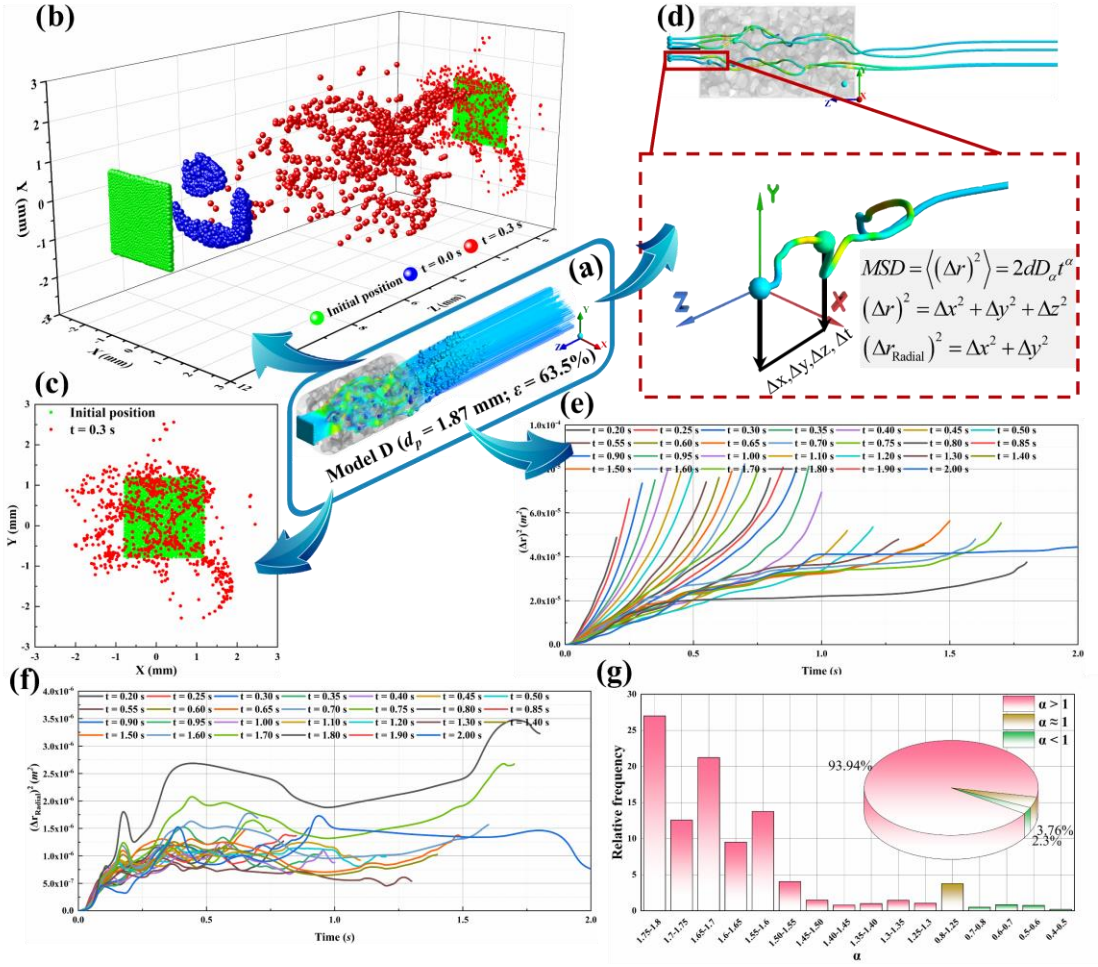

FIGURE 7 Characterization of fluid flow in foam channels. (a) The dispersion of tracked particles on streamlines that pass through a 2 mm square at the inlet of the foam model; (b) global and (c) radial dispersion: Green marker - Particle position tracked as it crosses the plane. Blue marker - particle touched the foam surface, t = 0 s. Red marker - particle position tracked after 0.3 s; (d) Radial and global dispersion characterization of fluid elements in single streamline based on mean square displacement theory; (e) Global dispersion with different residence times; (f) Radial dispersion with different residence times; (g) The frequency distribution of fluid element in foam media, where the goodness of fit $R^2 = 0.99$. $0.8 < \alpha < 1.25$ are considered as normal dispersion (brown pattern), and others are sub- dispersion (green pattern) and super- dispersion (pink pattern), respectively.

Defining the flow characteristics inside the foam channels is the key to study the effect of flow and dispersion on the reaction in the open-cell foam as catalyst substrate. If the fluid flow in the foam channels is stable, the motion trajectory of the fluid elements coincides with the streamline, and the parameter on the streamline (i.e., The spatial coordinates, time, velocity, etc. of the tracer particles on the streamline) can present the flow characteristics of the fluid element in the foam

medium. Therefore, a square plane of 2 mm × 2 mm was established at 2 mm above the foam cylinder, and 2000 streamlines were generated through this plane based on the simulation results. Moreover, making the streamline not touch the tube wall as much as possible to change the original streamline direction, so that these streamlines can reflect the fluid flow characteristics in the foam channels (in Figure 7a). Exporting the streamline data and analyzing the streamline data on the Matlab platform. Figure 7b shows the analysis of 2000 streamlines reaching the foam structure (shown by the blue ball), which is set as t = 0. When the fluid element in each streamline travels for 0.3 s, the position it reaches is shown by the red ball. After projecting it on the XY plane, the radial dispersion after 0.3 s is obtained, as shown in Figure 7c. We can find that the foam struts divide the spatial domain into multiple continuous penetrating cells, which facilitates better global and radial dispersion of the internal fluid element. How to clearly represent the fluid dispersion behavior in the complex foam cells is crucial for understanding the fluid transport and mixing in the foam channels. Therefore, this study is based on the mean square displacement theory in molecular dynamics to analyze the update motion behavior of the fluid element in the foam channels (in Figure 7d, see SI for the detailed process). Then we obtain the global and radial mean square displacement (in Equation s 27 – 28) of the streamlines in each time segment as a function of time (in Figures 7e, f). We can find that the time the fluid flows through the foam channel is different, and its dispersion behavior in the foam cell is also different. The global dispersion weakens as the consuming time, and the radial dispersion is less law due to the stretching and folding of the fluid elements [15]. Therefore, based on Equation 29, the optimal dispersion coefficient D_α and time term power α of the global diffusive are obtained. The frequency distribution of α is shown in Figure 6g. It can be

found that the fluid dispersion inside the foam channel belongs to a kind of super dispersion behavior ($\alpha > 1$), its dispersion coefficient of 10^{-4} m^2/s^{α} (in Figure S2) far exceeds the molecular diffusion coefficient (10^{-5} m^2/s). This also shows that the open-cell foam structure contributes to enhancing mass transfer-limited reactions under laminar flow conditions.

$$\left(\Delta r\right)^2 = \frac{1}{m}\sum_{n=i}^{n=m}\left[\left(x_i - x_0\right)^2 + \left(y_i - y_0\right)^2 + \left(z_i - z_0\right)^2\right] \tag{27}$$

$$\left(\Delta r_{Radial}\right)^2 = \frac{1}{m}\sum_{n=i}^{n=m}\left[\left(x_i - x_0\right)^2 + \left(y_i - y_0\right)^2\right] \tag{28}$$

$$MSD = \left\langle \left(\Delta r\right)^2 \right\rangle = D_{\alpha} t^{\alpha} \tag{29}$$

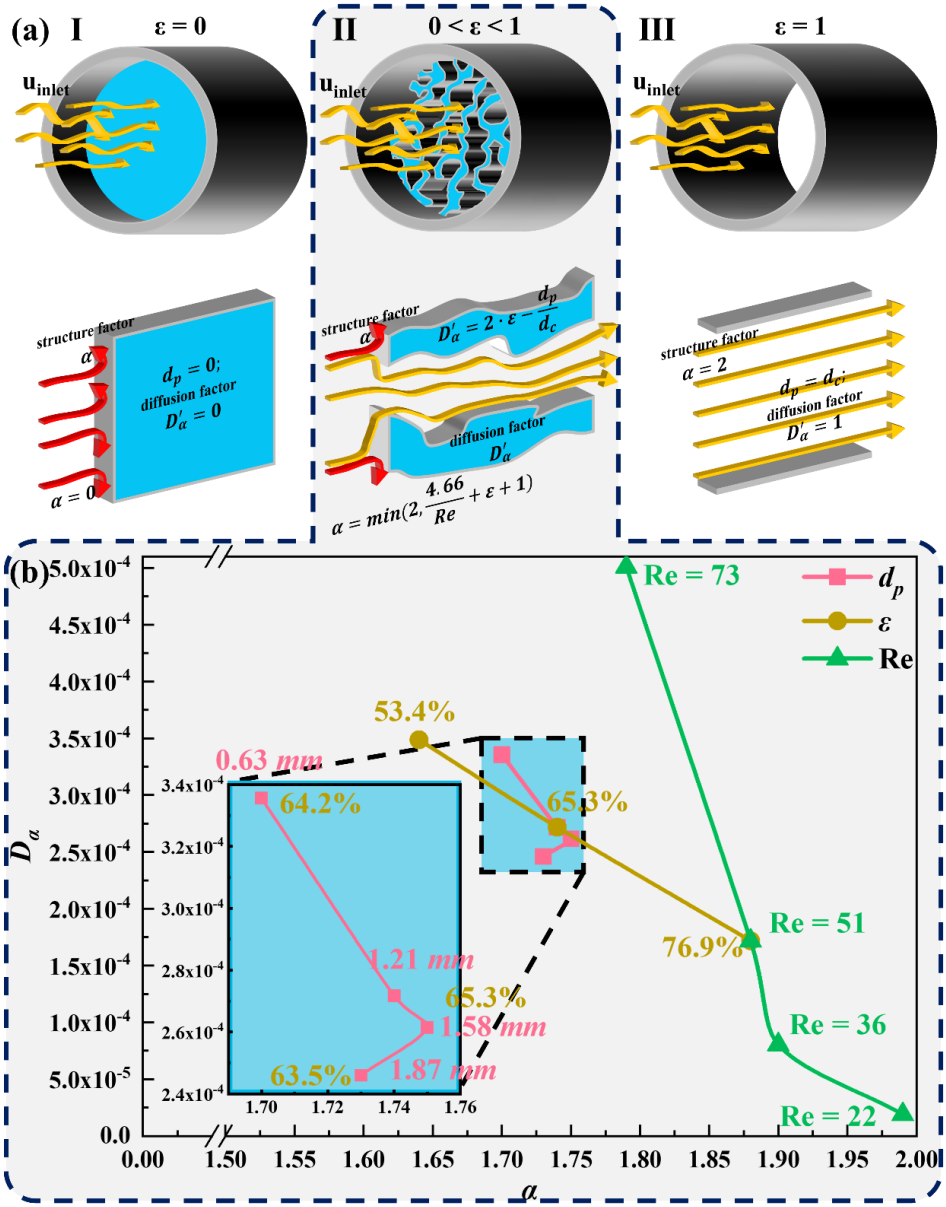

FIGURE 8 (a) Schematic diagram of the flow and dispersion mechanism in foam media; (b) The distribution for D_α and α under different porous structures (d_p and ε) and Re.

How to conceptualize the flow and dispersion inside the foam channels based on the foam structure and flow parameters is very meaningful for understanding species transport, mixing, and reaction. In Figure. 6e, f, we can find that the evolution laws of $(\Delta r)^2$ and $(\Delta r_{Radial})^2$ depends on residence times in foam part. However, the number of streamlines with too long or too short residence time accounts for a small proportion and can be ignored (in Figure. S4). Therefore, we selected the time period with the largest proportion of residence time as the reference streamline

data of foam structure (that is, the time period of red column in Figure S4, the number of streamlines is more than 800, accounting for more than 40%). The time interval is 0.0001s, and the corresponding ΔX, ΔY, ΔZ of different times are obtained. The corresponding $\left(\Delta r\right)^2$ and $\left(\Delta r_{Radial}\right)^2$ of different foam structures are obtained by the Equations (27) and (28). Moreover, discussing the variation law of the mean square displacement under different foam structures ((d_p and ε)) and Reynolds numbers (see the support information section 3 for details, in Figures S3 – S6). The distribution for D_a and a under different d_p, ε, and Re as shown in Figure 8b. The pink, brown and green markers in the Figure 8b represent the best fit D_a and a of the d_p, ε, and Re, respectively. We find that decreasing Re or increasing d_p or ε lead to a decrease in both D_a and a. This shows that the foam structure parameters (mean d_p and ε) and flow parameters (Re at inlet) can characterize the mean square displacement, and there is a function with D_a and a. When $\varepsilon = 0$, the channel is blocked by obstacles and the fluid cannot pass, $\left\langle \left(\Delta r\right)^2 \right\rangle = 0$ (in Figure 8a (I)). When $\varepsilon = 1$, there is no obstacle in the channel, ignoring the influence of wall effect, $\left\langle \left(\Delta r\right)^2 \right\rangle = \left(u_{inlet} \cdot t\right)^2$ (in Figure 8a (III)). When $0 < \varepsilon < 1$, the fluid passes through the foam channels with the mean pore size d_p and the mean porosity ε, the ε determines the fluid obstruction effect caused by the part of the foam strut. The Re determines the strength of the obstruction effect, and this obstruction effect in the foam channel is mainly in the form of super dispersion ($1 < \alpha < 2$, in Figure 6 g). α satisfies Equation 30. Meanwhile, the mean d_p and ε also affect the dispersion, and the column diameter (d_c) determines the degree of the effect of the d_p. So D_α satisfies Equation 31 (in Figure 8a (II)). The best constants A, B and C obtained by fitting are 4.66, 2 and 1, respectively (The error between the calculated Da and a of the fitting and the simulated Da and a is less than 5%, as shown in Figure

S7). Therefore, the conceptual equation of the mean square displacement (in Equation 32) of the fluid element flow in the foam medium is established. We call the α ($\alpha = \min\left(2, \frac{4.66}{\mathrm{Re}} + \varepsilon + 1\right)$) that affects the form of dispersion structure factor. $D_\alpha^{'}$ ($D_\alpha^{'} = \left(2 \cdot \varepsilon - \frac{d_p}{d_c}\right)$), which affects the dispersion, is called the dispersion factor. Then when $\varepsilon = 0$, its $d_p = 0$, $D_\alpha^{'} = 0$ and $\alpha = 0$, which satisfies the completely blocked tube channel condition (in Equation 33). When $\varepsilon = 1$, its $d_p = d_c$, $D_\alpha^{'} = 1$ and $\alpha = 2$, which also satisfies the completely open tube channel (in Equation 34). This shows that this conceptual equation is closed and reasonable. In addition, the structure factor and dispersion factor in this process are all the results after comprehensive analysis based on a large number of streamlines. These streamlines can show the flow law in foam channels, which has universal law under the same foam structure characteristics.

$$\alpha = \min\left(2, \frac{A}{\mathrm{Re}} + \varepsilon + 1\right) \tag{30}$$

$$D_\alpha = D_\alpha^{'} \cdot u_{inlet}^{\alpha} = \left(B \cdot \varepsilon - C\frac{d_p}{d_c}\right) \cdot u_{inlet}^{\alpha} \tag{31}$$

$$\left\langle (\Delta r)^2 \right\rangle = \left(2 \cdot \varepsilon - \frac{d_p}{d_c}\right)\left(u_{inlet} \cdot t\right)^{\min\left(2, \frac{4.66}{\mathrm{Re}} + \varepsilon + 1\right)} \tag{32}$$

$$\varepsilon = 0, \Rightarrow \begin{cases} d_p = 0 \\ D_\alpha^{'} = 0 \\ \alpha = 1 \end{cases} \tag{33}$$

$$\varepsilon = 1, \Rightarrow \begin{cases} d_p = d_c \\ D_\alpha^{'} = 1 \\ \alpha = 2 \end{cases} \tag{34}$$

5.4 velocity distribution

The flow and dispersion inside the foam medium will further affect the velocity distribution of the fluid in the foam cells. Moreover, the velocity distribution is critical to the reaction residence time of the fluid in the structured catalyst. We all know that open-cell foams shrink the fluid, thus causing the increase in the flow velocity in the foam channels. Figures 9a,c,e show the variation of normed mean velocity (area-weighted values, $u^* = u/u_{inlet}$) along the Z-axis (inlet velocity direction) under different Re, d_p, and ε. Figure 9b,d,f show the velocity distributions in the XZ-plane (this plane parallel to the flow direction) for different Re, d_p, and ε. We can find that the fluid velocity in the open-cell foam channels is closely related to the foam structure. Its velocity is increased by 40% - 270%. The maximum mean velocity difference Δu^* of the XY plane in the porous channel is 0.13 under laminar flow in Figure 9a, the velocity distribution is narrow and u^* is less dependent on the inlet velocity (u_{inlet}). In Figure 9b, it can be found that Re < 73 is obviously in the Darcy regime, and the velocity from the center of the channel to the wall has a gradual variety from the maximum value to zero. When the ε is similar and the d_p is different, the increase of u^* is basically the same, but its Δu^* is quite different. The smaller the d_p, the smaller its Δu^* (in Figure 9c). As shown in Figure 9d, with d_p increases, the more uneven of the cross-sectional pore distribution, the larger its Δu^*. With similar d_p and different ε, the smaller the ε, the larger the increase of u^* and the lager the Δu^* (in Figure 9e). As shown in Figure 9f, when the ε increases, its Δu^* decreases significantly. It is worth noting that Δu^* is very critical for the stretching and folding of the fluid element in the porous channel and the chemical reaction gradient [15]. Interestingly, the dispersion factor, $D_\alpha^{'}$, can perfectly represent the evolution law of the velocity difference inside the foam medium. With d_p increases and ε decreases, $D_\alpha^{'}$ decreases and Δu^* increases. This also shows that

the larger the $D_{\alpha}^{'}$, the smaller the Δu^{*}, the more helpful the homogeneous dispersion.

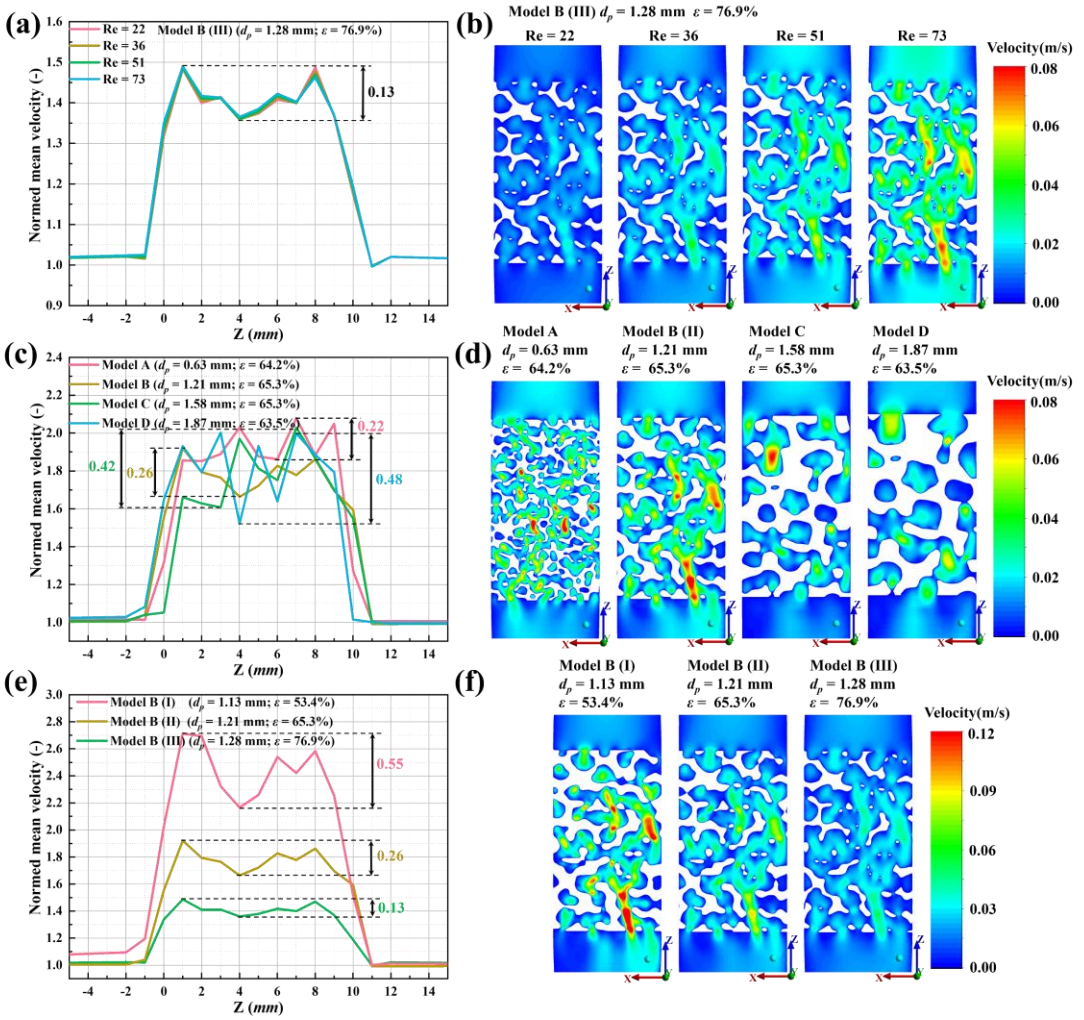

FIGURE 9 (a) Normed area-weighted average velocities along the z direction under different Re; (b) Velocity distribution of the XZ-plane in a porous channel under different Re; (c) Normed area-weighted average velocities along the z direction under different d_p; (d) Velocity distribution of the XZ-plane in a porous channel under different d_p; (e) Normed area-weighted average velocities along the z direction under different d_p; (f) Velocity distribution of the XZ-plane in a porous channel under different d_p.

5.5 Pressure drop distribution

The pressure gradient across the foam is related to the foam geometry, fluid properties, and flow conditions. The increase of Re (in Figure 10a), the decrease of ε (in Figure 10b), and the decrease of d_p (in Figure 10c) will cause the increase of pressure drop. The most common modelling method for describing the pressure drop in a packed bed and porous media is Darcy-Forchheimer (in Equation 35).

$$\frac{\Delta P}{L}=\frac{1}{K}\mu u+\frac{1}{\Gamma}\rho u^2 \tag{35}$$

where K and Γ are Darcy and non-Darcy permeability. These parameters are closely related to the geometric properties of porous media. At present, the Ergun equation[36] and the pressure drop equation[37] (in Equation 36) proposed by Kozeny based on the assumption of spherical particles are widely used.

$$\frac{\Delta P}{L}=\frac{(1-\varepsilon)}{\varepsilon^3}\left(\frac{A^{'}(1-\varepsilon)}{d_{par}^2}\mu u+\frac{B^{'}}{d_{par}}\rho u^2\right) \tag{36}$$

where $A^{'}$ is the viscous coefficient and $B^{'}$ is the inertial coefficient, which are 150 and 1.75, respectively. However, the foam structure is significantly different from the packed bed, and the assumption based on a uniform spherical shape obviously does not apply to the foam structure. Therefore, this paper introduces the structure factor (α) by analogy to Equation 37, and proposes the following expression for the pressure gradient.

$$\frac{\Delta P}{L}=\frac{2-\alpha}{(\alpha-1)^3}\left(\frac{A}{d_p^2}\mu u+\frac{B}{d_p}\rho u^2\right) \tag{37}$$

The optimal A and B obtained by fitting are 412 and 4.3, respectively. The comparison of model predictions and simulated $\Delta P/L$ is shown in Figure 9d. We can find that this model is more predictive than Bracconi's model[3], Kozeny's model [37]. This also shows that the structural factor (α) in this conceptual model (in Equation 32) can be used as a key factor to present the variation law of foam pressure drop.

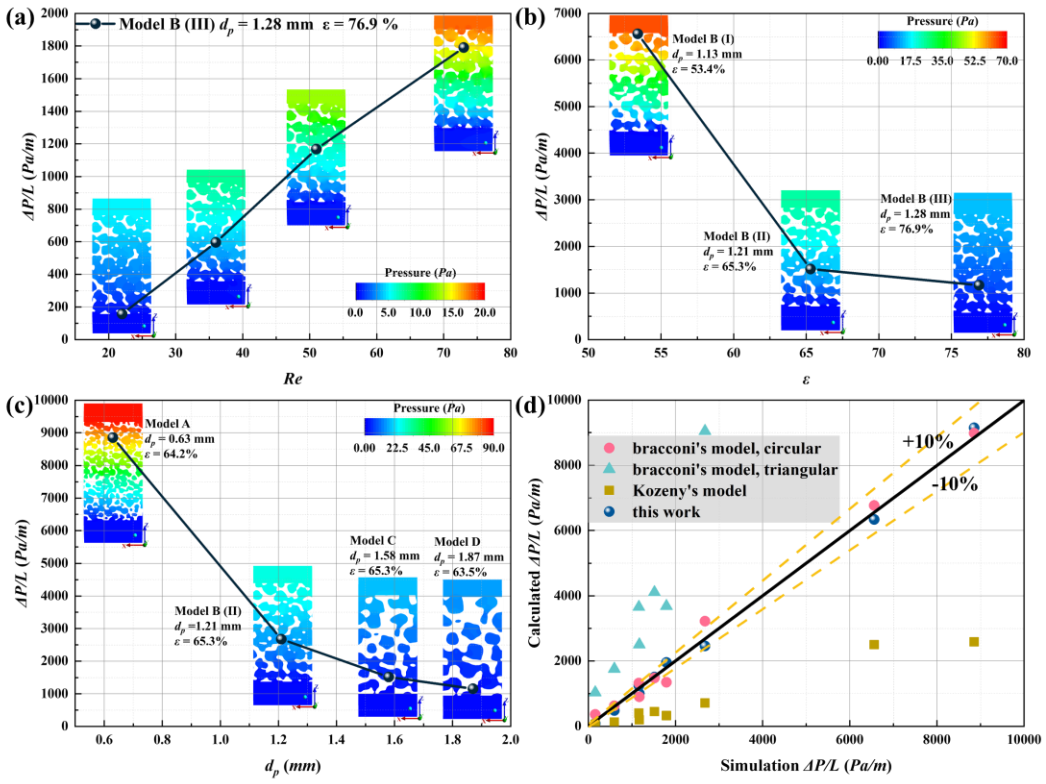

FIGURE 10 The evolution of $\Delta P/L$ with (a) Re, (b) ε, and (c) d_p; (d) Comparison of simulation $\Delta P/L$ and calculated $\Delta P/L$ of Bracconi's model[3], Kozeny's model [37], and this work.

5.6 Reaction kinetics

The flow and dispersion forms in the foam cells can affect the reaction kinetics, but the effect mechanism has always been a difficult point in this field, resulting in the limited scale-up of the catalytic process based on foam substrates. In this section, the influence laws and characteristics of foam structure (ε and d_p, in Figure 11a,b), flow conditions (Re, in Figure 11c), temperature (T, in Figure 11d), and molar ratio (R_m, in Figure 11e) on 'the conversion of LA are discussed, and then the mechanism of its influence on reaction kinetics is presented. We found that decreasing Re, ε, or d_p, or increasing T, or R_m all help to increase the α_{LA} after the LA and EtOH flow through the foam medium. In 2021, Ding et al. [31] proposed the following modeling scheme, and introduced the impact

factor λ into the equation of the original reaction rate, the detailed expression is shown in Equations 38 and 39.

$$k_{f,r}^{'} = \lambda^{a} k_{f,r} \tag{38}$$

$$k_{H_2O}^{'} = \lambda^{b} k_{H_2O} \tag{39}$$

where $k_{f,r}^{'}$ is constant of the forward reaction rate, $k_{H_2O}^{'}$ is the constant of water adsorption equilibrium, λ is the impact factor (dimensionless number, in Table S1), and a and b are correlation coefficients, -0.783 and -0.392, respectively. For the plug flow reaction process, the impact factor, λ is mainly determined by the flow form constructed by the foam struts. The conceptual dispersion model of the foam structure perfectly interprets the flow characteristics of the foam segment. Therefore, the structure factor and dispersion factor are introduced in the impact factor (in Equation 40). C_2 in the equation is 0.103 [38], and C_1, m, and n are fitted with optimal constants of 0.16, 5, and 1, respectively. The comparison between the calculated value, λ and the experimental value [31] is shown in Figure 11(f), and it can be found that the prediction model is in good agreement with the experimental results (The error is less than 5%). Moreover, we found that the larger the $D_{\alpha}^{'}$, the better the dispersion, the larger the λ, the more favorable the reaction, the larger the α, the larger the porosity, the larger the reaction volume, and the larger the λ, the more favorable the reaction. This shows that this kinetic model explains the influence mechanism from the flow and dispersion characteristics in the foam cells, and provides a reaction kinetics prediction model for the catalytic reaction process based on the foam substrate.

$$\lambda = C_1 \cdot \alpha^{m} \cdot \left(D_{\alpha}^{'}\right)^{n} + C_2 \ln R_m = 0.16\alpha^{5} D_{\alpha}^{'} + 0.103 \ln R_m \tag{40}$$

$$R = \frac{\lambda^{-0.783} k_{f,r}\left(\alpha_{LA}\alpha_{EtOH} - \alpha_{EL}\alpha_{H_2O}/K_e\right)}{\left(1+\lambda^{-0.392} k_{H_2O}\alpha_{H_2O}\right)^2} \tag{41}$$

$$\alpha_i = \gamma_i \frac{C_i}{C_{total}} \tag{42}$$

$$k_{H_2O} = 6.144\times10^{-10} \exp\left(-\frac{46996.215}{RT}\right) \tag{43}$$

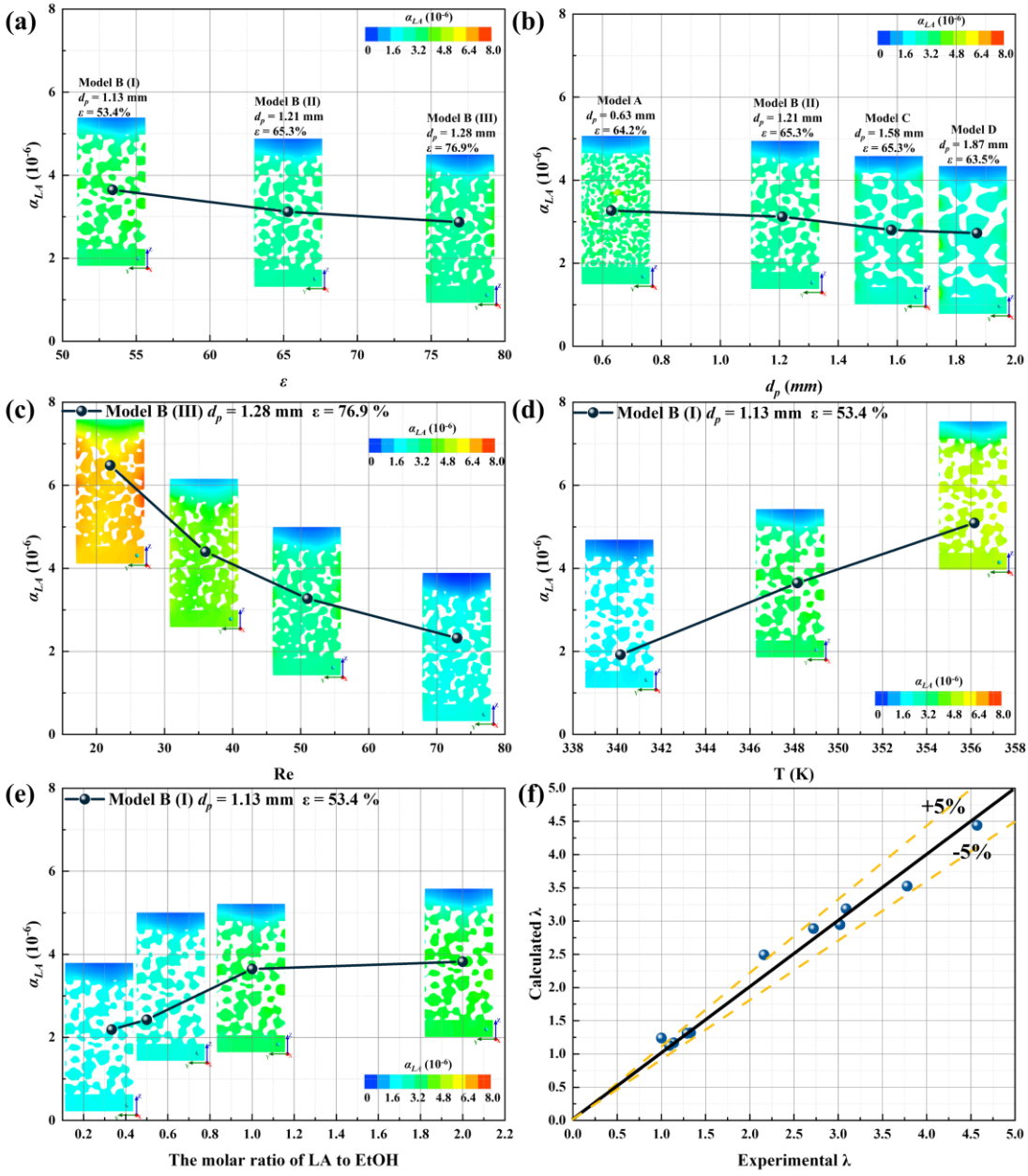

FIGURE 11 The conversion of LA at outlet with (a) ε, (b) d_p, (c) Re, (d) temperature (T), and (e) the molar ratio of LA to EtOH (R_m); (f) Comparison of experimental λ and calculated λ.

6. Conclusions

In this paper, the realistic foam structure is obtained based on the μ-CT, the effects of foam structure (ε and d_p), flow conditions (Re), the molar ratio of LA to EtOH (R_m), and temperature (T) on the fluid flow, dispersion, and reaction in the foam channel are studied based on the surface reaction. The following conclusions are shown:

Firstly, based on the microscopic mean square displacement theory, the flow and dispersion laws of the fluid in the foam channels were found from the perspective of fluid elements. A conceptual model that defines the motion characteristics of fluid elements inside the foam channel is proposed. Moreover, we found that the dispersion factor ($D_{\alpha}^{'}$) and structure factor (α) in this model can perfectly represent the variation law of velocity difference and pressure drop inside the foam channels. Finally, a reaction kinetic model based on the dispersion characteristics of fluid elements in the foam channels is proposed. This model is good consistent with the experimental results. This also provides a reaction kinetics prediction model for the catalytic reaction process with the foam substrate.

Acknowledgments

The authors are grateful for the financial support from the National Key R&D Program of China (2019YFE0123200), the National Natural Science Foundation of China (Nos. 22178249, 22222809) and the Haihe Laboratory of Sustainable Chemical Transformations. The authors also thank the reviewers for their insightful comments and suggestions.

Nomenclature

α_i the molar conversion of species i

C	molar concentration, **mol/L**
d_H	characteristic length
d_p	pore diameter
d_{par}	particle diameter
d_I	integral length scale
$D_{i,m}$	the mass diffusion coefficient for species i in the mixture
$D_{T,i}$	the thermal diffusion coefficient
$M_{w,i}$	the molecular weight of species i
p_{abs}	the absolute pressure
k_B	the Boltzmann constant (1.38×10^{-23} J/molecule-K)
$\mathbf{g}$	gravitational acceleration, **m/s²**
P	system pressure, **MPa**
R_m	molar ratio of LA to EtOH
Re	Reynolds number
Re_p	Pore-scale Reynolds number
Y_i	The mass fraction of species i
T_{ref}	Reference temperature, **K**
$\vec{J}_j$	the diffusion flux of species
λ	the impact factor
λ_e	the effective conductivity
u	velocity, **m/s**
μ	viscosity, **mPa·s**
σ	surface tension, **N/m**

ρ	density, **kg/m^3**

Abbreviations

CFD	computational fluid dynamics
CSF	continuous surface force
PISO	pressure implicit with splitting of operators

Subscripts

i	species i
inlet	inlet position
LA	levulinic acid
EtOH	ethanol
EL	ethyl levulinate
H_2O	water

References

1. Barreto G, Canhoto P, Collares-Pereira M. Three-dimensional CFD modelling and thermal performance analysis of porous volumetric receivers coupled to solar concentration systems. *Applied Energy*. 2019;252doi:10.1016/j.apenergy.2019.113433
2. Bianchi E, Heidig T, Visconti CG, Groppi G, Freund H, Tronconi E. Heat transfer properties of metal foam supports for structured catalysts: Wall heat transfer coefficient. *Catalysis Today*. 2013;216:121-134. doi:10.1016/j.cattod.2013.06.019
3. Bracconi M, Ambrosetti M, Okafor O, et al. Investigation of pressure drop in 3D replicated open-cell foams: Coupling CFD with experimental data on additively manufactured foams. *Chemical Engineering Journal*. 2019;377doi:10.1016/j.cej.2018.10.060
4. Shu C, Li X, Li H, Gao X. Design and optimization of reactive distillation: a review. *Frontiers of Chemical Science and Engineering*. 2022:1-20.
5. Li H, Yi F, Li X, Gao X. Numerical modeling of mass transfer processes coupling with reaction for the design of the ozone oxidation treatment of wastewater. *Frontiers of Chemical Science and Engineering*. 2020;doi:10.1007/s11705-020-1963-4
6. Martín-Sómer M, Pablos C, de Diego A, et al. Novel macroporous 3D photocatalytic foams for simultaneous wastewater disinfection and removal of contaminants of emerging concern. *Chemical Engineering Journal*. 2019;366:449-459. doi:10.1016/j.cej.2019.02.102
7. Egaña A, Sanz O, Merino D, Moriones X, Montes M. Fischer–Tropsch Synthesis Intensification in Foam Structures. *Industrial & Engineering Chemistry Research*. 2018;57(31):10187-10197. doi:10.1021/acs.iecr.8b01492

8. Peng P-Y, Jin I, Yang TCK, Huang C-M. Facile preparation of hierarchical CuO–CeO2/Ni metal foam composite for preferential oxidation of CO in hydrogen-rich gas. *Chemical Engineering Journal*. 2014;251:228-235. doi:10.1016/j.cej.2014.04.077
9. Ou X, Pilitsis F, Jiao Y, et al. Hierarchical Fe-ZSM-5/SiC foam catalyst as the foam bed catalytic reactor (FBCR) for catalytic wet peroxide oxidation (CWPO). *Chemical Engineering Journal*. 2019;362:53-62. doi:10.1016/j.cej.2019.01.019
10. Jiao Y, Xu S, Jiang C, Perdjon M, Fan X, Zhang J. MFI zeolite coating with intrazeolitic aluminum (acidic) gradient supported on SiC foams to improve the methanol-to-propylene (MTP) reaction. *Applied Catalysis A: General*. 2018;559:1-9. doi:10.1016/j.apcata.2018.04.006
11. Wood BD, He X, Apte SV. Modeling Turbulent Flows in Porous Media. *Annual Review of Fluid Mechanics*. 2020;52(1):171-203. doi:10.1146/annurev-fluid-010719-060317
12. Ergun S. Fluid flow through packed columns. *Journal of Materials Science and Chemical Engineering*. 1952;48(2):89-94.
13. Dybbs A, Edwards RV. *A New Look at Porous Media Fluid Mechanics — Darcy to Turbulent*. Springer Netherlands; 1984.
14. Kaviany, M. *[Mechanical Engineering Series] Principles of Heat Transfer in Porous Media*. 1995.
15. Heyman J, Lester DR, Turuban R, Meheust Y, Le Borgne T. Stretching and folding sustain microscale chemical gradients in porous media. *Proc Natl Acad Sci U S A*. Jun 16 2020;117(24):13359-13365. doi:10.1073/pnas.2002858117
16. Turuban R, Lester DR, Le Borgne T, Meheust Y. Space-Group Symmetries Generate Chaotic Fluid Advection in Crystalline Granular Media. *Phys Rev Lett*. Jan 12 2018;120(2):024501. doi:10.1103/PhysRevLett.120.024501
17. Aref H, Blake JR, Budišić M, et al. Frontiers of chaotic advection. *Reviews of Modern Physics*. 2017;89(2)doi:10.1103/RevModPhys.89.025007
18. Kolmogorov, A., N. The Local Structure of Turbulence in Incompressible Viscous Fluid for Very Large Reynolds Numbers. *Proceedings of the Royal Society A: Mathematical*. 1991;434(1890):9-13.
19. Kundu, PijushK. *Fluid mechanics / 4th ed*. Fluid mechanics / 4th ed; 2010.
20. Ottino JM. The kinematics of mixing: stretching, chaos, and transport. *Cambridge & New York Cambridge University Press P*. 2011;
21. Stroock, Abraham D, Derringer, et al. Chaotic Mixer for Microchannels. *Science*. 2002;
22. Avila-Marin AL, Fernandez-Reche J, Martinez-Tarifa A. Modelling strategies for porous structures as solar receivers in central receiver systems: A review. *Renewable and Sustainable Energy Reviews*. 2019;111:15-33. doi:10.1016/j.rser.2019.03.059
23. Bracconi M, Ambrosetti M, Maestri M, Groppi G, Tronconi E. A systematic procedure for the virtual reconstruction of open-cell foams. *Chemical Engineering Journal*. 2017;315:608-620. doi:10.1016/j.cej.2017.01.069
24. Bracconi M, Ambrosetti M, Maestri M, Groppi G, Tronconi E. A fundamental investigation of gas/solid mass transfer in open-cell foams using a combined experimental and CFD approach. *Chemical Engineering Journal*. 2018;352:558-571. doi:10.1016/j.cej.2018.07.023
25. Das S, Deen NG, Kuipers JAM. Direct numerical simulation for flow and heat transfer through

random open-cell solid foams: Development of an IBM based CFD model. *Catalysis Today*. 2016;273:140-150. doi:10.1016/j.cattod.2016.03.048

26. Fan X, Ou X, Xing F, et al. Microtomography-based numerical simulations of heat transfer and fluid flow through β -SiC open-cell foams for catalysis. *Catalysis Today*. 2016;278:350-360. doi:10.1016/j.cattod.2015.12.012

27. Sinn C, Pesch GR, Thöming J, Kiewidt L. Coupled conjugate heat transfer and heat production in open-cell ceramic foams investigated using CFD. *International Journal of Heat and Mass Transfer*. 2019;139:600-612. doi:10.1016/j.ijheatmasstransfer.2019.05.042

28. Della Torre A, Lucci F, Montenegro G, et al. CFD modeling of catalytic reactions in open-cell foam substrates. *Computers & Chemical Engineering*. 2016;92:55-63. doi:10.1016/j.compchemeng.2016.04.031

29. Dong Y, Korup O, Gerdts J, Roldán Cuenya B, Horn R. Microtomography-based CFD modeling of a fixed-bed reactor with an open-cell foam monolith and experimental verification by reactor profile measurements. *Chemical Engineering Journal*. 2018;353:176-188. doi:10.1016/j.cej.2018.07.075

30. Wehinger GD, Heitmann H, Kraume M. An artificial structure modeler for 3D CFD simulations of catalytic foams. *Chemical Engineering Journal*. 2016;284:543-556. doi:10.1016/j.cej.2015.09.014

31. Ding Q, Li H, Chen Z, et al. Kinetics and design of distillation reactor with ZSM-5@ SiC foam catalytic packing for EL synthesis in industrial scale. *Authorea Preprints*. 2021;

32. Gao X, Ding Q, Wu Y, et al. Kinetic study of esterification over structured ZSM-5-coated catalysts based on fluid flow situations in macrocellular foam materials. *Reaction Chemistry & Engineering*. 2020;5(3):485-494. doi:10.1039/c9re00445a

33. Li H, Fu L, Li X, Gao X. Mechanism and analytical models for the gas distribution on the SiC foam monolithic tray. *AIChE Journal*. 2015;61(12):4509-4516. doi:doi:10.1002/aic.14944

34. McGee HA. *Molecular engineering*. McGraw-Hill; 1991.

35. Yang P, Li X, Li H, Cong H, Kiss AA, Gao X. Unraveling the influence of residence time distribution on the performance of reactive distillation – Process optimization and experimental validation. *Chemical Engineering Science*. 2021;237doi:10.1016/j.ces.2021.116559

36. Ergun S, Orning AA. Fluid flow through randomly packed columns and fluidized beds. *Industrial & Engineering Chemistry*. 1949;41(6):1179-1184.

37. Kozeny J. Uber kapillare leitung der wasser in boden. *Royal Academy of Science, Vienna, Proc Class I*. 1927;136:271-306.

38. Gao X, Li X, Li H. Hydrolysis of methyl acetate via catalytic distillation: Simulation and design of new technological process. *Chemical Engineering and Processing: Process Intensification*. 2010;49(12):1267-1276. doi:10.1016/j.cep.2010.09.015